JACS
JOURNAL OF THE AMERICAN CHEMICAL SOCIETY
Article
pubs.acs.org/JACS

Rapid Proton-Detected NMR Assignment for Proteins with Fast Magic Angle Spinning

Emeline Barbet-Massin,[†] Andrew J. Pell,[†] Joren S. Retel,[‡] Loren B. Andreas,[†,§] Kristaps Jaudzems,[∥] W. Trent Franks,[‡] Andrew J. Nieuwkoop,[‡] Matthias Hiller,[‡] Victoria Higman,[‡] Paul Guerry,[†] Andrea Bertarello,[†] Michael J. Knight,[†] Michele Felletti,[†] Tanguy Le Marchand,[†] Svetlana Kotelovica,[⊥] Inara Akopjana,[⊥] Kaspars Tars,[⊥] Monica Stoppini,[#] Vittorio Bellotti,[#,▽] Martino Bolognesi,[○] Stefano Ricagno,[○] James J. Chou,[◆] Robert G. Griffin,[§] Hartmut Oschkinat,[‡] Anne Lesage,[†] Lyndon Emsley,[†] Torsten Herrmann,[†] and Guido Pintacuda*[,†]

[†]Centre de RMN à Très Hauts Champs, Institut des Sciences Analytiques (CNRS, ENS Lyon, UCB Lyon 1), Université de Lyon, 69100 Villeurbanne, France

[‡]Leibniz-Institut für Molekulare Pharmakologie, 13125 Berlin, Germany

[§]Francis Bitter Magnet Laboratory and Department of Chemistry, Massachusetts Institute of Technology, Cambridge, Massachusetts 02139, United States

[∥]Latvian Institute of Organic Synthesis, Riga LV-1006, Latvia

[⊥]Biomedical Research and Study Centre, Riga LV-1067, Latvia

[#]Department of Molecular Medicine, University of Pavia, 65 Pavia, Italy

[▽]Wolfson Drug Discovery Centre National Amyloidosis Centre, Centre for Amyloidosis and Acute Phase Proteins, University College London (UCL), London WC1E 6BT, U.K.

[○]Department of Biosciences, University of Milano, 20126 Milano, Italy

[◆]Harvard Medical School, Boston, Massachusetts 02115, United States

Supporting Information

ABSTRACT: Using a set of six ^{1}H-detected triple-resonance NMR experiments, we establish a method for sequence-specific backbone resonance assignment of magic angle spinning (MAS) nuclear magnetic resonance (NMR) spectra of 5−30 kDa proteins. The approach relies on perdeuteration, amide ^{2}H/^{1}H exchange, high magnetic fields, and high-spinning frequencies ($\omega_r/2\pi \geq 60$ kHz) and yields high-quality NMR data, enabling the use of automated analysis. The method is validated with five examples of proteins in different condensed states, including two microcrystalline proteins, a sedimented virus capsid, and two membrane-embedded systems. In comparison to contemporary ^{13}C/^{15}N-based methods, this approach facilitates and accelerates the MAS NMR assignment process, shortening the spectral acquisition times and enabling the use of unsupervised state-of-the-art computational data analysis protocols originally developed for solution NMR.

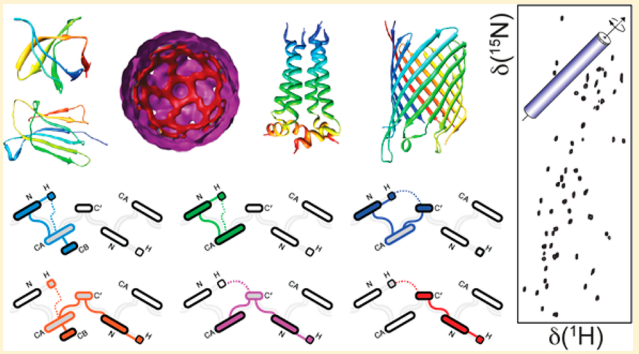

INTRODUCTION

In the last 15 years, magic angle spinning (MAS) NMR emerged as a generally applicable structural biology technique, complementing liquid-state NMR, X-ray crystallography, and electron microscopy. Following seminal work on microcrystalline proteins,[1,2] examples demonstrating the utility of MAS include studies of prion fibrils,[3,4] polydisperse full-size heat shock complexes,[5] intact viral capsids,[6] membrane-bound drug targets,[7,8] and bacterial virulence factors[9,10] at an atomic level. Approaches for sample preparation, sequence-specific resonance assignment, and collection of conformational restraints have been designed to calculate three-dimensional structures and to determine their dynamics. However, these procedures are still far from routine, and therefore, the development of a robust, rapid, and general protocol is needed for MAS NMR to become a widespread, universal tool in structural biology, for the novice as well as the expert. In particular, sequence-specific resonance assignment of MAS spectra remains the prerequisite

Received: July 21, 2014
Published: August 7, 2014

   dx.doi.org/10.1021/ja507382j | J. Am. Chem. Soc. 2014, 136, 12489−12497

for site-specific studies that yield internuclear distances, torsion angles, and molecular structures.

Currently, MAS NMR assignment procedures are primarily based on double- and triple-resonance spectra, making use of correlations between ^{13}C and ^{15}N signals.[11,12] These procedures usually require large amounts (~1 mg/kDa) of $^{13}C/^{15}N$ labeled samples, long data acquisition times, and expert manual analysis of the spectra. This is in contrast to the standard solution NMR acquisition and analysis protocols, where established triple-resonance pulse schemes correlating backbone and side chain ^{1}H, ^{13}C, and ^{15}N resonances are used for sequential assignment.[13] These heteronuclear approaches have been used in thousands of solution NMR studies, and in general, they provide high-quality data that allow the use of modern, error-tolerant computational algorithms and protocols for efficient and objective data analysis with minimal human intervention.[14,15]

Due to its high gyromagnetic ratio and natural abundance, ^{1}H is the optimal choice for detection in solution. In solids, however, these same properties are responsible for a network of strong homonuclear ^{1}H dipolar couplings that dramatically lower the resolution. To observe high-resolution ^{1}H signals in solids, the homogeneous broadening characteristic of this network[16] needs to be overcome, by dilution of the proton content in the sample[17,18] and/or by fast sample spinning[19,20] in conjunction with high magnetic fields.

In proteins, proton dilution can be controlled easily by expression in perdeuterated media followed by reintroduction of protons at exchangeable sites. Resolved spectra were demonstrated on a deuterated protein sample with full protonation of the amide sites at the MAS rate of 20 kHz,[21] and a further improvement in resolution was achieved by Reif's and Rienstra's groups, respectively, by lowering the levels of amide protonation (typically 10−40%)[22−25] or by increasing the MAS rates up to 40 kHz,[26] a spinning regime where well-resolved spectra can be obtained even in fully protonated small proteins.[27] Under these conditions, ^{1}H detection can be combined with assignment protocols based on dipolar-assisted $^{15}N/^{13}C$ and $^{13}C/^{13}C$ correlations.[28,29] More recently, we have shown that high-quality proton-detected cross-polarization-based $^{15}N-^{1}H$ correlations ("CP-HSQC") that maintain simultaneously high sensitivity and high resolution can be obtained at spinning frequencies $\omega_r/2\pi \geq 60$ kHz for fully back-protonated, deuterated samples.[30,31] In this spinning regime, long ^{13}C and ^{15}N coherence lifetimes are observed with application of low power ^{1}H decoupling,[32−34] and scalar coupling interactions become viable for efficient homonuclear ^{13}C transfer, similar to solution NMR. This has opened the way to new, expeditious backbone resonance assignment strategies for significantly larger proteins and to the rapid detection of structurally relevant parameters.[35−37]

Here we show that in this regime, sensitive high resolution solution-NMR-like $^{15}N-^{1}H$ protein fingerprint spectra can be recorded on a wide variety of proteins and sample preparations. This leads to well-dispersed signals in an optimized suite of 3D spectra for rapid de novo assignment of medium-sized microcrystalline proteins, sedimented particles, and membrane-integrated systems. Notably, the NMR spectra are of sufficient quality for performing automated and robust sequence-specific backbone resonance assignment using a modern computational data analysis program.[38]

EXPERIMENTAL SECTION

Sample Preparation. All [100%$^{1}H^{N}$,^{2}H,^{13}C,^{15}N]-labeled samples were expressed in deuterated minimal media, and all refolding and reconstitution steps were performed in buffers containing 100% H_2O, to obtain samples that are fully protonated in the exchangeable sites. Samples were concentrated and packed into the NMR rotor, by using microcrystallization protocols,[12,39] sedimentation,[40−43] or detergent dialysis into phospholipid membranes.[44,45] Details on each sample preparation are provided in the Supporting Information (SI).

NMR Data Acquisition. All spectra were recorded on Bruker Avance III 800 or 1000 spectrometers operating at Larmor frequencies of 800 or 1000 MHz for ^{1}H, at 60 kHz MAS using triple-resonance HCN 1.3 mm probes. The temperature of the sample was regulated using a VT gas flow in the range of 230−243 K, in order to achieve an estimated sample temperature of 300 K.

In the 2D CP-HSQC spectra (Figure 1), the nonselective 90° pulses were set to 2.5 μs at 100 kHz rf-field amplitude (^{1}H), 5.0 μs at 50 kHz rf-field amplitude (^{15}N), and 3.12 μs at 80 kHz rf-field amplitude (^{13}C). $^{1}H-^{15}N$ forward cross-polarization (CP) was achieved using a contact time of 1.5 ms, during which the ^{1}H rf-field amplitude was ramped linearly from 12 to 30 kHz, and the ^{15}N rf-field amplitude was held constant at 38 kHz. The $^{15}N-^{1}H$ back CP was achieved using a contact time of 0.4 ms, during which the ^{1}H rf-field amplitude was ramped linearly from 29 to 11 kHz, and the ^{15}N rf-field amplitude was held constant at 39 kHz. The swept-low-power TPPM sequence[47] or the WALTZ-16 sequence[48] were found to be equally effective for ^{1}H-heteronuclear decoupling during t_1, while WALTZ-16 was used for ^{13}C and ^{15}N decoupling during ^{1}H acquisition. Swept-low-power TPPM was applied with a two-pulse phase difference of 41°, a pulse length that was linearly ramped from 40 to 26.67 μs in steps of −1.33 μs, and an rf-field amplitude of 13.7 kHz. WALTZ-16 was applied at 10 kHz rf-field amplitude. The MISSISSIPPI pulse sequence[46] was used without homospoil gradients to suppress the water signal, with a 19 kHz irradiation for 100−300 ms. All the spectra were acquired and processed using the States-TPPI procedure.[49] CP-HSQCs were acquired with between 8 and 16 scans, with 160−400 increments in the indirect ^{15}N dimension, giving total experimental times of between 25 min and 1.5 h (see Table S1 in the SI).

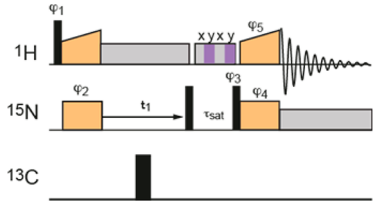

Figure 1. Pulse sequence for the ^{1}H-detected $^{15}N-^{1}H$ 2D correlation ("CP-HSQC"). Narrow and broad black rectangles indicate $\pi/2$ and π-pulses, respectively. Orange boxes indicate cross-polarization, and gray boxes indicate heteronuclear decoupling. The MISSISSIPPI sequence[46] is indicated by the striped box. All pulses are of phases 0, unless indicated differently. $\varphi1$ = 1 3, $\varphi2$ = 1, $\varphi3$ = 0 0 2 2, $\varphi4$ = 1, $\varphi5$ = {1}*4 {3}*4, φrec = 1 3 3 1 3 1 1 3.

For the six 3D experiments of Figure 3, the experimental parameters were as described for the CP-HSQC. In addition, the initial CP sequence from H to CA/CO had contact times between 3 and 5 ms, with the rf amplitude on ^{1}H ramped linearly from 70 to 100 kHz (1 GHz) or from 90 to 100 kHz (800 MHz spectrometer) and a constant-amplitude ^{13}C spin lock of either 40 kHz (ZQ CP) or 15−20 kHz (DQ CP).[50] Both the CO−N and CA—N CP steps had a contact time between 8 and 15 ms with a constant-amplitude spin lock of about 35 kHz on ^{13}C and a tangent-modulated amplitude spin lock of mean rf-field amplitude of about 25 kHz on ^{15}N. The scalar CO−CA coherence transfer of the (H)CO(CA)NH experiment[31] comprised two spin echoes with half-echo delays τ of duration 4.7 and 4.0 ms for the CO and CA sides of the transfer, respectively. Gaussian-cascade Q3 frequency-selective refocusing pulses[51] were used during the

dx.doi.org/10.1021/ja507382j | J. Am. Chem. Soc. 2014, 136, 12489−12497

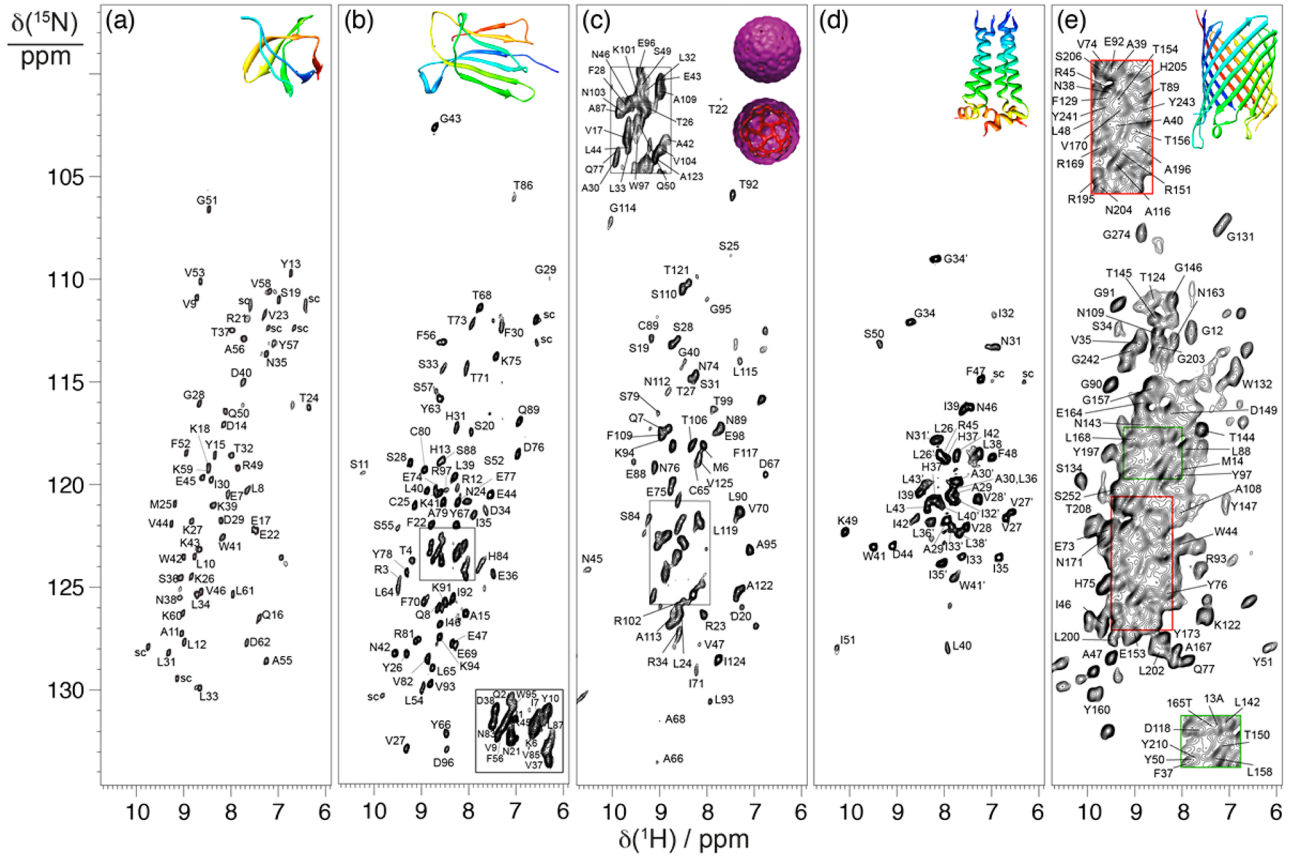

Figure 2. $^{15}N-^{1}H$ correlation spectra recorded on a 1 GHz spectrometer under 60 kHz MAS for [U-H^N,^2H,^{13}C,^{15}N]-labeled (a) microcrystalline SH3, (b) microcrystalline β2m, and (c) sedimented nucleocapsids of AP205, (d) M2 channel, and (e) OmpG.

second spin echo: the CO-selective pulse was of length 350 μs and rf-field peak amplitude 10 kHz, and the CA-selective pulse was of length 600 μs and rf-field peak amplitude 5.75 kHz. The (H)(CO)CA(CO)NH experiment[52] comprised two spin echoes for the out-and-back CO−CA scalar transfer, of which the half-echo was 4.7 ms. Both the (H)(CA)CB(CA)NH[52] and (H)(CA)CB(CACO)NH experiments used two spin echoes for the out-and-back CA—CB transfer, with Q3 refocusing pulse selective for the entire ^{13}C aliphatic region of length 150 μs, rf-field peak amplitude 20 kHz, and half-echo delays of 7.2 ms. In the (H)(CA)CB(CACO)NH experiment, the second scalar transfer from CA to CO was performed using the same parameters as for the (H)(CO)CA(CO)NH sequence. All spectra were acquired and processed using the States-TPPI method[49] in the indirect dimensions to obtain pure-phase line shapes and frequency discrimination. Codes and reference parameter sets for Bruker Avance III spectrometers are available on http://perso.ens-lyon.fr/guido.pintacuda/NMR.

Computational Protocol for Automated Resonance Assignment. An improved version of MATCH[38] was used to automatically obtain sequence-specific backbone assignment of the different protein data sets. MATCH employs local optimization for tracing partial sequence-specific assignments within a global, population-based search environment, where the simultaneous application of local and global optimization heuristics guarantees high efficiency and robustness of the results.[38] An identical calculation protocol was applied to all protein data sets. MATCH used as input the amino acid sequence of the protein, a statistical analysis of chemical shift values of proteins contained in the BioMagResBank, and the experimental input data of the six solid-state triple-resonance NMR experiments in the form of frequency coordinates of the manually identified NMR signals. First, the input listings of the NMR signals were automatically consolidated and transformed into a set of spin systems, containing all available intra- and inter-residual chemical shifts for a given unassigned protein residue. The inevitable presence of spectral artifacts and spectral overlap in the experimental data induce ambiguity and uncertainties into the sequential as well as the sequence-specific information. In order to deal with such ambiguities, MATCH accounts for the fact that each spin system may exist in multiple states; i.e., a spin system is allowed to be degenerate. For this process of spin system assembly, large proton and nitrogen chemical shift matching tolerances of 0.05 and 0.5 ppm were used, respectively. Second, sequential connectivity of spin systems was then simultaneously established by MATCH via the three intra- and inter-residual CA, CB, and CO resonances using a carbon chemical shift matching tolerance of 0.5 ppm. After these two initialization steps of the algorithm, the genetic optimization process of MATCH was started in order to find the best possible solution to the assignment problem. For each protein data set, 10 independent optimization runs were performed, and sequence-specific resonance assignments which occur in more than 50% of the optimization runs were accepted as being correct and yielded the final list of assigned resonance frequencies. The overall calculation time was in all cases below 5 min on a single CPU of a contemporary Mac desktop equipped with a dual-core Intel Core i5 processor. The new version of MATCH is available free-of-charge for the academic community as a submodule of the UNIO application suite. Download information is available under http://perso.ens-lyon.fr/torsten.herrmann/Software.

RESULTS AND DISCUSSION

Figure 2 shows the CP-HSQC of five different proteins acquired at 1 GHz ^1H Larmor frequency with $\omega_r/2\pi$ = 60 kHz. Figure 2a,b corresponds to microcrystalline proteins, namely, the α-spectrin (SH3) domain[53] and β2-microglobulin, the light chain of the class I major histocompatibility complex (β2m),[54] Figure 2c to the sedimented viral nucleocapsid of *Acinetobacter* phage 205 (AP205),[55] and Figure 2d,e to α-helical and β-barrel membrane proteins, respectively, the conductance domain from influenza A M2[56] and the outer membrane protein G (OmpG)

dx.doi.org/10.1021/ja507382j | J. Am. Chem. Soc. 2014, 136, 12489−12497

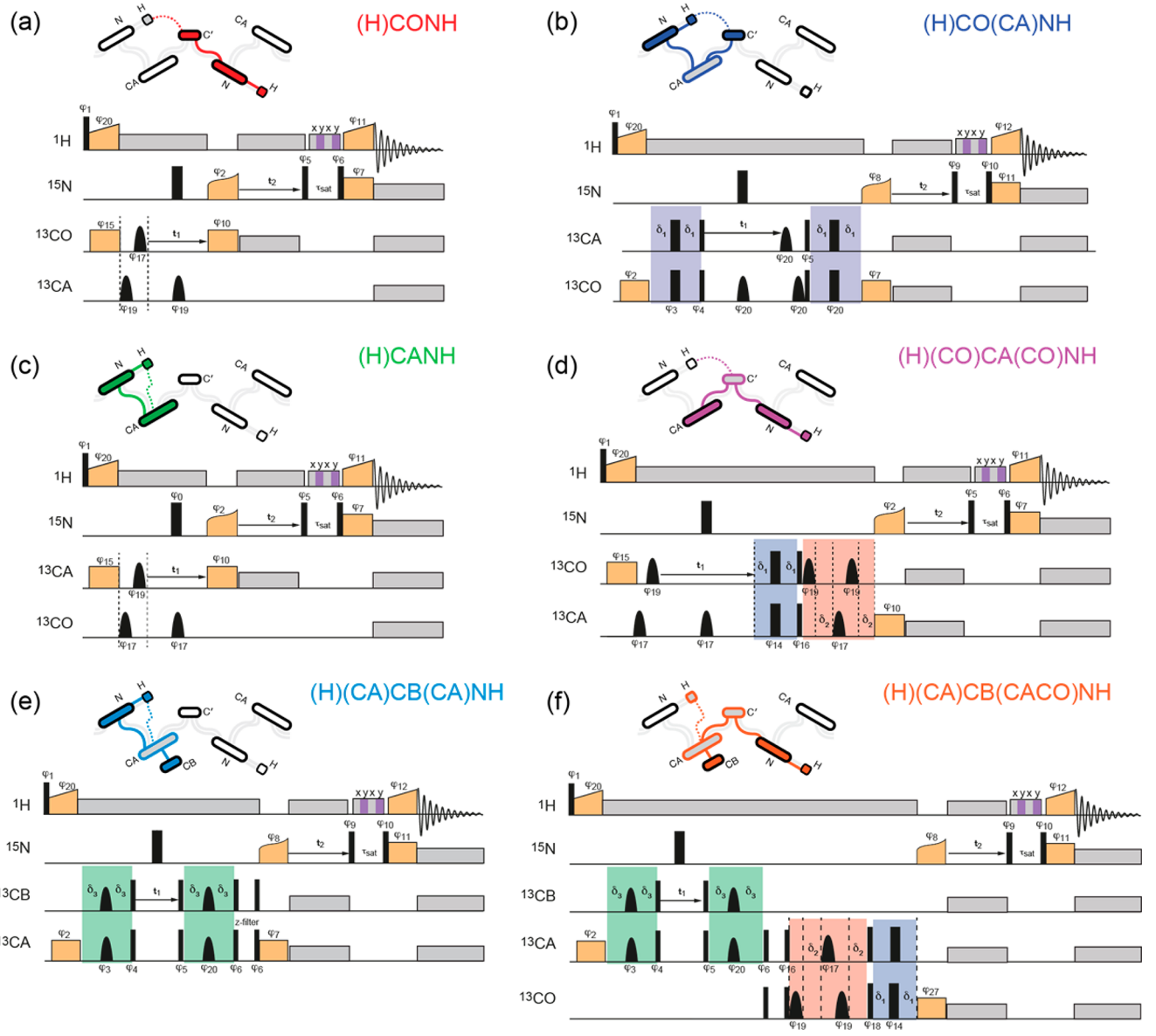

Figure 3. Pulse sequences for the six ^{1}H-detected ^{13}C−^{15}N−^{1}H 3D correlation experiments, with an illustration of the coherence transfers and spins involved: (a) inter-residue (H)CONH experiment ($CO_{i-1}N_iH_i$), (b) intraresidue (H)CO(CA)NH experiment ($CO_iN_iH_i$), (c) intraresidue (H)CANH experiment ($CA_iN_iH_i$), (d) inter-residue (H)(CO)CA(CO)NH experiment ($CA_{i-1}N_iH_i$), (e) intraresidue (H)(CA)CB(CA)NH experiment ($CB_iN_iH_i$), and (f) inter-residue (H)(CA)CB(CACO)NH experiment ($CB_{i-1}N_iH_i$). Narrow and broad black rectangles indicate $\pi/2$ and π pulses, respectively, and bell shapes represent selective inversion pulses. Orange boxes indicate cross-polarization, and gray boxes indicate heteronuclear decoupling. The MISSISSIPPI sequence is indicated by the striped box. Spin-echoes involved in the transfer between CO and CA are highlighted in blue and red, when the coherence is present on the CO and CA, respectively, and spin-echoes involved in transfer between CA and CB are highlighted in green. All pulses are of phases 0, unless indicated differently. (a and c) $\varphi1$ = 0 2, $\varphi20$ = 1, $\varphi2$ = 1, $\varphi6$ = 0 0 2 2, $\varphi12$ = 1, $\varphi7$ = 1, $\varphi11$ = {1}*4 {3}*4, φrec = 1 3 3 1 3 1 1 3; (b) $\varphi1$ = 0 2, $\varphi20$ = 1, $\varphi2$ = 1, $\varphi6$ = 0 0 2 2, $\varphi12$ = 1, $\varphi7$ = 1, $\varphi11$ = 1, $\varphi14$ = {0}*4 {1}*4, $\varphi17$ = {0}*8 {1}*8, φrec = 3 1 1 3 1 3 3 1 1 3 3 1 3 1 1 3; (d and e) $\varphi1$ = 1 3, $\varphi2$ = 1 1 3 3, $\varphi4$ = 1, $\varphi5$ = 1, $\varphi7$ = {1}*4 {3}*4, $\varphi8$ = {0}*8 {2}*8, $\varphi9$ = 3, $\varphi10$ = 1, φrec = 0 2 2 0 2 0 0 2 2 0 0 2 0 2 2 0; (f) $\varphi1$ = 1 3, $\varphi2$ = 1 1 3 3, $\varphi4$ = 1, $\varphi5$ = 1, $\varphi6$ = {0}*16 {2}*16, $\varphi9$ = 3, $\varphi10$ = 1, $\varphi14$ = {0}*8 {1}*8, $\varphi16$ = 3, $\varphi17$ = {0}*4 {1}*4, φrec = 0 2 2 0 2 0 0 2 2 0 0 2 0 2 2 0 2 0 0 2 0 2 2 0 0 2 2 0 2 0 0 2. Specific CP to or from ^{13}C may require a frequency shift, and in this case, the phases of rf during the two ^{13}C CP periods are aligned respectively at the end and at the beginning of the contact time. In the diagrams, filled circles denote spins for which the frequency of evolution is measured. Solid lines represent transfers between bonded nuclei and dashed lines between nonbonded nuclei.

from Gram-negative bacteria.[57] These spectra can be acquired with adequate signal-to-noise in 5−30 min using only 2−3 mg of sample. The spectra in Figure 2a−d exhibit ^{1}H line widths (FWHM) of approximately 50−100 Hz and ^{15}N line widths of 20−60 Hz.

These CP-HSQC spectra serve as an efficient module to build 3D triple-resonance correlation experiments. Simple 3D spectra correlating ^{1}H, ^{15}N, and the neighboring ^{13}CO/^{13}CA, such as (H)CONH and (H)CANH (parts a and c of Figure 3, respectively), can be built with two heteronuclear ^{1}H/^{13}C and ^{15}N/^{13}C cross-polarization steps followed by the ^{15}N/^{1}H transfer from the CP-HSQC.[26]

More complex experiments can be obtained by the addition of homonuclear carbon−carbon *J*-based coherence transfer

dx.doi.org/10.1021/ja507382j | J. Am. Chem. Soc. 2014, 136, 12489−12497

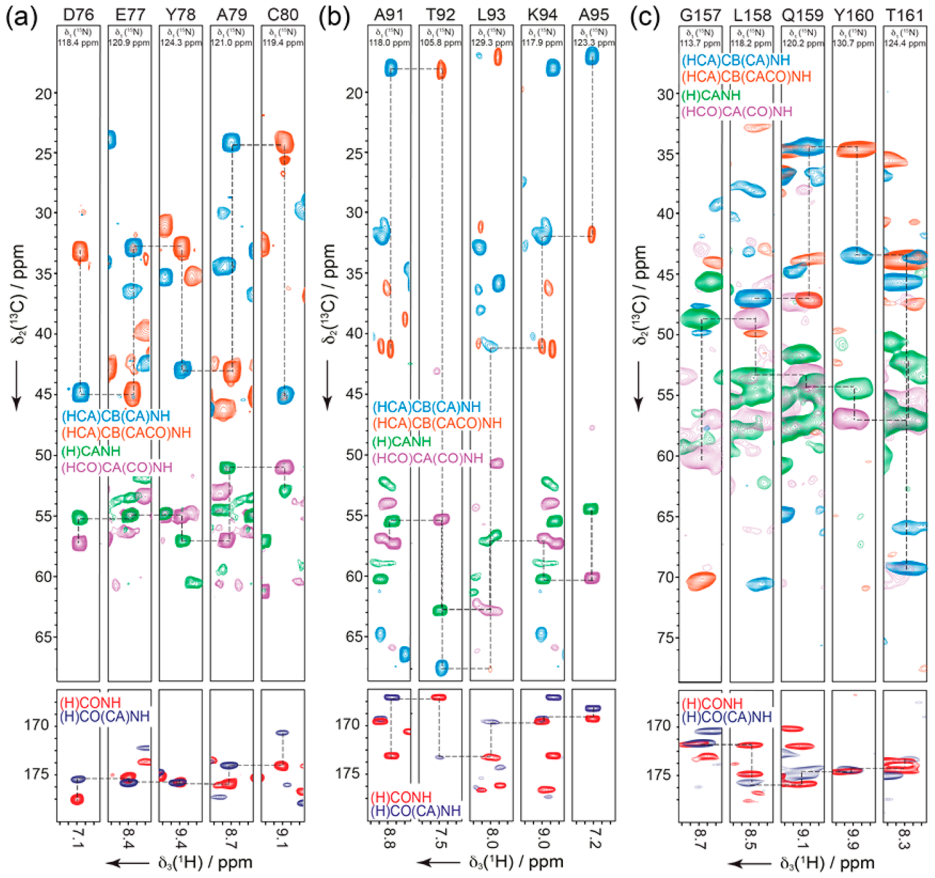

Figure 4. Strip plots of both inter- and intraresidue CB, CA, and CO resonances for NH pairs in β2m (a), AP205 (b), and OmpG (c).

blocks, enabled by the long ^{13}C coherence lifetimes obtainable at 60 kHz MAS. One, two (out-and-back), or three carbon−carbon transfers result in the (H)CO(CA)NH (Figure 3b),[31] (H)(CO)CA(CO)NH and (H)(CA)CB(CA)NH (Figure 3d and e),[52] and (H)(CA)CB(CACO)NH experiments (Figure 3f), respectively. This latter is a newly designed pulse sequence and is crucial for the exploitation of the CB shifts in the backbone resonance assignment (see below).

Figure 4a−c illustrates sequence-specific resonance assignments obtained by joint analysis of the set of six spectra. Simultaneous matching of three independent ^{13}C (CO, CA, and CB) chemical shifts that are correlated with ^{1}H and ^{15}N nuclei from adjacent residues yields a high level of redundancy for establishing sequential connectivity. This is realized stepwise: first, CA and CB chemical shifts of each spin system allow for a rough classification of the residue type, and second, a robust sequential matching of spin systems is established. Fragments of three and more sequentially connected spin systems can then usually be unambiguously matched to the protein sequence. Following cross-peak selection, these steps may be quickly performed interactively by an experienced spectroscopist or by application of computational backbone assignment algorithms. This latter possibility is an attractive feature that is essential to accelerate the data analysis and to render the procedure more impartial. For each protein automatically investigated by MATCH, we first interactively generated peak lists of NMR resonance signals from the six NMR experiments and subjected them together with the protein sequence to a modified version of the program UNIO-MATCH.[38] Contrary to contemporary computer-aided protocols tailored for the analysis of ^{13}C-detected MAS NMR data, this routine benefits from direct application of road-proven protocols developed for solution NMR.[58−61] In particular, MATCH is able to directly make use of the individual input peak lists, in contrast to many automated backbone resonance assignment routines that require (tedious and subjective) manual assembly of the spin systems, and is robust with respect to the inclusion of erroneous, artifactual NMR signals that might be present in the input peak lists. The new version of UNIO-MATCH used here automatically performs spin system assembly and residue typing and exploits a memetic optimization algorithm to find the optimal solution for sequence-specific resonance assignment.

Here we report the backbone resonance assignments of the five proteins (see SI for chemical shift lists). Resonance assignments were automatically obtained and validated interactively for all data sets, except for OmpG. OmpG presented an extremely challenging data analysis task that turned out to be most reliably done by interactive analysis.

For the crystalline proteins, 52 and 75 backbone amide cross-peaks were automatically assigned for the SH3 domain (62 residues) and β2m (99 residues), respectively. For both proteins, this corresponds to 100% of the observed backbone H^N−N resonances in the 2D CP-HSQC (Figure 2a,b), where prolines and flexible or disordered parts such as N- and C-terminal tails are absent. Both proteins show long transverse coherence lifetimes (~20 and 45 ms, respectively for ^{13}CA and ^{13}CO); hence, efficient magnetization transfers are guaranteed also in the experiments with multiple ^{13}C homonuclear

dx.doi.org/10.1021/ja507382j | J. Am. Chem. Soc. 2014, 136, 12489−12497

Table 1. Experimental Performance of the Assignment Strategy for the Five Proteins[a]

	SH3	β2m	AP205	M2	OmpG
residues (prolines)	62 (2)	99 (5)	130 (8)	2 × 43 (1)	281 (8)
		CP-HSQC			
$S/N/\sqrt{t}$	32.3	31.2	14.8	17.6	45.0
experimental time for $(S/N)_i > 4$	1.6 min	3.2 min	25 min	3.2 min	16 min
actual experimental time	1 h	1 h	1 h, 30 min	1 h	25 min
scans per increment	8	8	16	8	8
N_iH_i peaks	52	75	95	44	–
		(H)CANH			
sensitivity wrt HSQC (first FID)	0.32	0.24	0.20	0.32	0.31
experimental time for $(S/N)_i > 4$	30 min	2 h	21 h, 30 min	1 h, 10 min	6 h, 30 min
actual experimental time	1 h, 15 min	6 h, 25 min	11 h	1 h, 30 min	1 d, 21 h, 30 min
scans per increment	2	4	16	2	64
$CA_iN_iH_i$ peaks	52	75	94	44	251
		(H)(CO)CA(CO)NH			
sensitivity wrt HSQC (first FID)	0.19	0.13	0.16	0.09	0.11
experimental time for $(S/N)_i > 4$	1 h, 25 min	6 h, 30 min	1 d, 9 h	15 h	2 d, 1 h
actual experimental time	2 h, 30 min	13 h	22 h	2 d	2 d, 1 h
scans per increment	4	8	32	64	128
$CA_{i-1}N_iH_i$ peaks	50	71	83	43	167
		(H)(CA)CB(CA)NH			
sensitivity wrt HSQC (first FID)	0.16	0.11	0.14	0.06	0.07
experimental time for $(S/N)_i > 4$	2 h	9 h, 10 min	1 d, 21 h	1 d, 9 h	1 d, 6 h*
actual experimental time	7 h, 30 min	12 h, 30 min	22 h	2 d	1 d, 40 min
scans per increment	4	8	32	64	64
$CB_iN_iH_i$ peaks	51	72	71	42	128
		(H)(CA)CB(CACO)NH			
sensitivity wrt HSQC (first FID)	0.13	0.07	0.08	0.03	0.03
experimental time for $(S/N)_i > 4$	3 h	22 h, 30 min	5 d, 18 h	5 d, 13 h	6 d, 21 h*
actual experimental time	15 h	1 d, 1 h	2 d, 16 h	7 d, 10 h	4 d, 6 h, 25 min
scans per increment	8	16	96	232	128
$CB_{i-1}N_iH_i$ peaks	49	62	61	30	106
		(H)CONH			
sensitivity wrt HSQC (first FID)	0.35	0.30	0.24	0.25	0.29
experimental time for $(S/N)_i > 4$	25 min	1 h, 20 min	14 h, 50 min	2 h	7 h
actual experimental time	1 h	1 h, 45 min	6 h	3 h	1 d, 6 h
scans per increment	2	4	8	4	32
$CO_{i-1}N_iH_i$ peaks	52	71	92	44	185
		(H)CO(CA)NH			
sensitivity wrt HSQC (first FID)	0.12	0.08	0.11	0.08	0.05
experimental time for $(S/N)_i > 4$	3 h, 30 min	17 h, 30 min	2 d, 23 h	19 h	2 d, 12 h*
actual experimental time	8 h	14 h	1 d, 12 h	2 d, 2 h	2 d, 15 h, 45 min
scans per increment	16	32	48	64	64
$CO_iN_iH_i$ peaks	50	75	69	40	89
assigned residues	52	75	94	44	112

[a]The table reports the sensitivity ($S/N/\sqrt{t}$) of the CP-HSQC, calculated on the integral of the first increment, acquired for 20 ms, after 20 Hz of exponential apodization (120 Hz in the case of OmpG), as well as the estimated experimental times necessary to achieve a S/N per peak $[(S/N)_p] > 4$. The corresponding number of scans (ns) per increment necessary was calculated according to the following relation[62]

$$\left(\frac{S}{N}\right)_p = \left(\frac{S/N}{\sqrt{t}}\right)_{HSQC} \frac{1}{p}\frac{T_2^*(N)}{t_{1max}}\left(1 - e^{-t_{1max}/T_2^*(N)}\right)\sqrt{ns \times ni(N)t} \geq 4$$

assuming a $T_2^*(N)$ of 6.3 ms and 48 (ni) increments (t_{1max} acquisition of a maximum of 5 ms) in the ^{15}N (t_1) indirect dimension, and t is the time required by a single scan. For each of the six 3D experiments, the relative sensitivity (rel sens) with respect to the CP-HSQC was calculated on the integral of the first increment, and the estimated number of scans ns per increment necessary to achieve a $(S/N)_p > 4$ was calculated according to the relation:

$$\left(\frac{S}{N}\right)_p = \left(\frac{S/N}{\sqrt{t}}\right)_{HSQC} \frac{\text{rel sens}}{p}\frac{T_2^*(N)}{t_{1max}}\frac{T_2^*(C)}{t_{2max}}\left(1 - e^{-t_{1max}/T_2^*(N)}\right)$$
$$\left(1 - e^{-t_{2max}/T_2^*(C)}\right)\sqrt{ns \times ni(N)\, ni(C)t} \geq 4$$

dx.doi.org/10.1021/ja507382j | J. Am. Chem. Soc. 2014, 136, 12489−12497

Table 1. continued

assuming a T_2* of 6.3 ms and 48 increments (t_{1max} and t_{2max} acquisitions of a maximum of 5 ms) for each ^{15}N (t_1) and ^{13}C (t_2) indirect dimension. t is the time required by a single scan, and p denotes the number of peaks, taken equal to the number of observed signals in the most sensitive and dispersed among the triple-correlation experiments, (H)CANH. (*) Experimental time necessary to achieve an average sensitivity per signal $(S/N)_p > 2$.

coherence transfers, allowing all six data sets to be recorded in 1.5 (SH3) and 2.5 (β2m) days (see Table 1).

For sedimented AP205, in which a homodimer of 2 × 130 residues assembles into an icosahedral particle of about 2.5 MDa,[55] the CP-HSQC spectrum shown in Figure 2c features a quality comparable to that of the two model microcrystalline samples. The six spectra were recorded in about 1 week, and backbone assignment was automatically determined for 94 residues (corresponding to all backbone resonances observed in the CP-HSQC and to 72% of the protein sequence).

Resonances from the N-terminus are not observed, and additional residues are likely to be absent due to incomplete unfolding during reprotonation.

Membrane-embedded systems are a challenging class of samples due to intrinsic heterogeneity, lipid dynamics, and limited protein content. The conductance domain M2 is a 5 kDa single pass transmembrane protein that assembles as a 20 kDa tetramer with a 10 kDa asymmetric dimer.[56] Although half of the sample mass consists of lipids, there is still excellent sensitivity in the spectrum of Figure 2d (obtained in 30 min), and the line widths (100 Hz for ^{1}H) are comparable to those of the crystalline models. For OmpG, several approaches to perform sequential assignments in lipid bilayers have been applied, including sparse and specific labeling and utilizing ^{13}C-detected experiments;[44] however, at 280 residues, this system remains a considerable challenge. The CP-HSQC spectrum of OmpG shown in Figure 2e displays excellent sensitivity characteristic of the ^{1}H-detected approach, as seen for the previous examples, despite the generally larger line widths (130−180 Hz). In these membrane protein cases, bulk ^{13}C coherence lifetimes of about 15−20 ms for both ^{13}CA and ^{13}CO result in some reduction of transfer efficiency (see Table 1). Nevertheless, the approach described above remains successful for the automatic assignment of M2 and of a considerable portions of OmpG by expert manual analysis, after acquisition of each set of six spectra in 14 days. In the case of M2, all 44 observed residues were assigned by MATCH constituting the transmembrane and amphipathic helices in the asymmetric dimer (26−51 and 26′−43′). As for OmpG, expert manual analysis yielded 40% overall assignment, corresponding to residues concentrated in the β-barrel; in the intracellular turns T1, T4, and T5; and in the extracellular loop L4, where crucial peaks for establishing inter-residue connectivities are most often missing.

A significant improvement in ^{13}C transverse relaxation was observed when increasing the MAS rates from 40 to 60 kHz. For the two microcrystalline proteins, about 30−50% longer bulk transverse coherence lifetimes were measured for ^{13}CA (15 vs 20 ms) and ^{13}CO (30 vs 45 ms), and a similar improvement was measured in the case of M2 (15−18 ms for ^{13}CA and 10−15 ms for ^{13}CO). Longer coherence lifetimes lead to improved transfer efficiencies (see, for example, Figure S1 in the SI), so we expect the assignment strategy described above to perform better at even higher MAS frequencies.

CONCLUSIONS

Our results from this diverse and challenging set of proteins demonstrate the excellent performance of the proposed standard suite of triple-resonance experiments for studies of proteins of different condensed states and show that modern, error-tolerant computational algorithms can be applied for the efficient and robust NMR data analysis. For microcrystalline and sedimented proteins, we find that the efficiencies of these experiments as compared to the basic ^{1}H-detected CP-HSQC experiment range from 0.5 for the (H)CONH and (H)CANH to 0.1 for the (H)(CA)CB(CACO)NH, while these efficiencies range from 0.32 to 0.03 for the membrane proteins. Acquisition times range from 36 h (SH3) to 2 weeks (M2 and OmpG) for the set of six spectra. The incorporation of an additional CB dimension accelerates and strengthens the reliability of backbone sequential assignment, and notably, triply redundant sequential chemical shift matching between intra- and inter-reside CA, CB, and CO resonances is the crucial component for the robustness of the procedure, using interactive or unsupervised methods alike. In the future, improved sensitivity, resolution, and coherence lifetimes are possible, for example, with the advent of probes with higher spinning frequencies, cryoprobes, or other advances, which will further improve the performance of the standard protocol proposed.

In conclusion, we were able to adapt and extend an experimental and computational protocol that is used extensively for solution protein NMR to address complex MAS spectra. In so doing, we have enlarged the sample repertoire accessible for assignment in solid-state NMR spectroscopy. This is a significant step toward routine structural investigations of large, poorly soluble, and noncrystalline systems.

ASSOCIATED CONTENT

Supporting Information

Sample preparation, curves with simulated efficiencies of the ^{13}C−^{13}C transfers in the different experiments, list of assigned chemical shifts, and pulse sequence code for Bruker spectrometers. This material is available free of charge via the Internet at http://pubs.acs.org.

AUTHOR INFORMATION

Corresponding Author

guido.pintacuda@ens-lyon.fr

Notes

The authors declare no competing financial interest.

ACKNOWLEDGMENTS

We thank Lénaïc Leroux for technical assistance with the NMR spectrometers. We acknowledge support from the Agence Nationale de la Recherche (ANR 10-BLAN-713-01), from Joint Research Activity and Access to Research Infrastructures, from a Marie-Curie ITN in the 7th FP of the EC (EAST-NMR no. 228461, BioNMR no. 261863, SMBP no. 211800), from the CNRS (TGIR-RMN-THC FR3050), from the Italian Ministry

of Research (grant FIRB RBFR109EOS), and from NIH (grants EB-001960 and EB-002026).

REFERENCES

(1) Castellani, F.; van Rossum, B.; Diehl, A.; Schubert, M.; Rehbein, K.; Oschkinat, H. *Nature* **2002**, *420*, 98−102.
(2) Rienstra, C. M.; Tucker-Kellogg, L.; Jaroniec, C. P.; Hohwy, M.; Reif, B.; McMahon, M. T.; Tidor, B.; Lozano-Perez, T.; Griffin, R. G. *Proc. Natl. Acad. Sci. U. S. A.* **2002**, *99*, 10260−10265.
(3) Wasmer, C.; Lange, A.; Van Melckebeke, H.; Siemer, A. B.; Riek, R.; Meier, B. H. *Science* **2008**, *319*, 1523−1526.
(4) Lu, J. X.; Qiang, W.; Yau, W. M.; Schwieters, C. D.; Meredith, S. C.; Tycko, R. *Cell* **2013**, *154*, 1257−1268.
(5) Jehle, S.; Rajagopal, P.; Bardiaux, B.; Markovic, S.; Kuhne, R.; Stout, J. R.; Higman, V. A.; Klevit, R. E.; van Rossum, B. J.; Oschkinat, H. *Nat. Struct. Mol. Biol.* **2010**, *17*, 1037−1042.
(6) Han, Y.; Ahn, J.; Concel, J.; Byeon, I. J. L.; Gronenborn, A. M.; Yang, J.; Polenova, T. *J. Am. Chem. Soc.* **2010**, *132*, 1976−1987.
(7) Lange, A.; Giller, K.; Hornig, S.; Martin-Eauclaire, M. F.; Pongs, O.; Becker, S.; Baldus, M. *Nature* **2006**, *440*, 959−962.
(8) Cady, S. D.; Schmidt-Rohr, K.; Wang, J.; Soto, C. S.; DeGrado, W. F.; Hong, M. *Nature* **2010**, *463*, 689−692.
(9) Shahid, S. A.; Bardiaux, B.; Franks, W. T.; Krabben, L.; Habeck, M.; van Rossum, B. J.; Linke, D. *Nat. Methods* **2012**, *9*, 1212−U1119.
(10) Loquet, A.; Sgourakis, N. G.; Gupta, R.; Giller, K.; Riedel, D.; Goosmann, C.; Griesinger, C.; Kolbe, M.; Baker, D.; Becker, S.; Lange, A. *Nature* **2012**, *486*, 276−279.
(11) Rienstra, C. M.; Hohwy, M.; Hong, M.; Griffin, R. G. *J. Am. Chem. Soc.* **2000**, *122*, 10979−10990.
(12) Böckmann, A.; Lange, A.; Galinier, A.; Luca, S.; Giraud, N.; Juy, M.; Heise, H.; Montserret, R.; Penin, F.; Baldus, M. *J. Biomol. NMR* **2003**, *27*, 323−339.
(13) Sattler, M.; Schleucher, J.; Griesinger, C. *Progr. NMR Spectrosc.* **1999**, *34*, 93−158.
(14) Guerry, P.; Herrmann, T. Q. *Rev. Biophys.* **2011**, *44*, 257−309.
(15) Serrano, P.; Pedrini, B.; Mohanty, B.; Geralt, M.; Herrmann, T.; Wüthrich, K. *J. Biomol. NMR* **2012**, *53*, 341−354.
(16) Maricq, M. M.; Waugh, J. S. *J. Chem. Phys.* **1979**, *70*, 3300−3316.
(17) Zheng, L.; Fishbein, K. W.; Griffin, R. G.; Herzfeld, J. *J. Am. Chem. Soc.* **1993**, *115*, 6254−6261.
(18) Reif, B.; Jaroniec, C. P.; Rienstra, C. M.; Hohwy, M.; Griffin, R. G. *J. Magn. Reson.* **2001**, *151*, 320−327.
(19) Samoson, A.; Tuherm, T.; Gan, Z. *Solid State Nucl. Magn. Reson.* **2001**, *20*, 130−136.
(20) Kobayashi, T.; Mao, K.; Paluch, P.; Nowak-Krol, A.; Sniechowska, J.; Nishiyama, Y.; Gryko, D. T.; Potrzebowski, M. J.; Pruski, M. *Angew. Chem., Int. Ed.* **2013**, *52*, 14108−14111.
(21) Paulson, E. K.; Morcombe, C. R.; Gaponenko, V.; Dancheck, B.; Byrd, R. A.; Zilm, K. W. *J. Am. Chem. Soc.* **2003**, *125*, 15831−15836.
(22) Chevelkov, V.; Rehbein, K.; Diehl, A.; Reif, B. *Angew. Chem., Int. Ed.* **2006**, *45*, 3878−3881.
(23) Linser, R.; Bardiaux, B.; Higman, V.; Fink, U.; Reif, B. *J. Am. Chem. Soc.* **2011**, *133*, 5905−5912.
(24) Linser, R.; Dasari, M.; Hiller, M.; Higman, V.; Fink, U.; del Amo, J. M. L.; Markovic, S.; Handel, L.; Kessler, B.; Schmieder, P.; Oesterhelt, D.; Oschkinat, H.; Reif, B. *Angew. Chem., Int. Ed.* **2011**, *50*, 4508−4512.
(25) Akbey, U.; Lange, S.; Franks, W. T.; Linser, R.; Rehbein, K.; Diehl, A.; van Rossum, B. J.; Reif, B.; Oschkinat, H. *J. Biomol. NMR* **2012**, *46*, 67−73.
(26) Zhou, D. H.; Shea, J. J.; Nieuwkoop, A. J.; Franks, W. T.; Wylie, B. J.; Mullen, C.; Sandoz, D.; Rienstra, C. M. *Angew. Chem., Int. Ed.* **2007**, *46*, 8380−8383.
(27) Zhou, D. H.; Shah, G.; Cormos, M.; Mullen, C.; Sandoz, D.; Rienstra, C. M. *J. Am. Chem. Soc.* **2007**, *129*, 11791−11801.
(28) Ward, M. E.; Shi, L.; Lake, E.; Krishnamurthy, S.; Hutchins, H.; Brown, L. S.; Ladizhansky, V. *J. Am. Chem. Soc.* **2011**, *133*, 17434−17443.
(29) Zhou, D. H.; Nieuwkoop, A. J.; Berthold, D. A.; Comellas, G.; Sperling, L. J.; Tang, M.; Shah, G. J.; Brea, E. J.; Lemkau, L. R.; Rienstra, C. M. *J. Biomol. NMR* **2012**, *54*, 291−305.
(30) Lewandowski, J. R.; Dumez, J. N.; Akbey, U.; Lange, S.; Emsley, L.; Oschkinat, H. *J. Chem. Phys. Lett.* **2011**, *2*, 2205−2211.
(31) Knight, M. J.; Webber, A. L.; Pell, A. J.; Guerry, P.; Barbet-Massin, E.; Bertini, I.; Felli, I. C.; Gonnelli, L.; Pierattelli, R.; Emsley, L.; Lesage, A.; Herrmann, T.; Pintacuda, G. *Angew. Chem., Int. Ed.* **2011**, *50*, 11697−11701.
(32) Laage, S.; Sachleben, J. R.; Steuernagel, S.; Pierattelli, R.; Pintacuda, G.; Emsley, L. *J. Magn. Reson.* **2009**, *196*, 133−141.
(33) Wickramasinghe, N. P.; Parthasarathy, S.; Jones, C. R.; Bhardwaj, C.; Long, F.; Kotecha, M.; Mehboob, S.; Fung, L. W. M.; Past, J.; Samoson, A.; Ishii, Y. *Nat. Methods* **2009**, *6*, 215−218.
(34) Lewandowski, J. R.; De Paëpe, G.; Eddy, M. T.; Struppe, J.; Maas, W.; Griffin, R. G. *J. Phys. Chem. B* **2009**, *113*, 9062−9069.
(35) Knight, M. J.; Pell, A. J.; Bertini, I.; Felli, I. C.; Gonnelli, L.; Pierattelli, R.; Herrmann, T.; Emsley, L.; Pintacuda, G. *Proc. Natl. Acad. Sci. U. S. A.* **2012**, *109*, 11095−11100.
(36) Marchetti, A.; Jehle, S.; Felletti, M.; Knight, M. J.; Wang, Y.; Xu, Z. Q.; Park, A. Y.; Otting, G.; Lesage, A.; Emsley, L.; Dixon, N. E.; Pintacuda, G. *Angew. Chem., Int. Ed.* **2012**, *51*, 10756−10759.
(37) Knight, M. J.; Felli, I. C.; Pierattelli, R.; Bertini, I.; Emsley, L.; Herrmann, T.; Pintacuda, G. *J. Am. Chem. Soc.* **2012**, *134*, 14730−14733.
(38) Volk, J.; Herrmann, T.; Wuthrich, K. *J. Biomol. NMR* **2008**, *41*, 127−138.
(39) Martin, R. W.; Zilm, K. W. *J. Magn. Reson.* **2003**, *165*, 162−174.
(40) Mainz, A.; Jehle, S.; van Rossum, B. J.; Oschkinat, H.; Reif, B. *J. Am. Chem. Soc.* **2009**, *131*, 15968−15969.
(41) Bertini, I.; Luchinat, C.; Parigi, G.; Ravera, E.; Reif, B.; Turano, P. *Proc. Natl. Acad. Sci. U. S. A.* **2011**, *108*, 10396−10399.
(42) Gardiennet, C.; Schutz, A. K.; Hunkeler, A.; Kunert, B.; Terradot, L.; Bockmann, A.; Meier, B. H. *Angew. Chem., Int. Ed.* **2012**, *51*, 7855−7858.
(43) Gelis, I.; Vitzthum, V.; Dhimole, N.; Caporini, M. A.; Schedlbauer, A.; Carnevale, D.; Connell, S. R.; Fucini, P.; Bodenhausen, G. *J. Biomol. NMR* **2013**, *56*, 85−93.
(44) Hiller, M.; Krabben, L.; Vinothkumar, K. R.; Castellani, F.; van Rossum, B. J.; Kuhlbrandt, W.; Oschkinat, H. *ChemBioChem.* **2005**, *6*, 1679−1684.
(45) Andreas, L. B.; Eddy, M. T.; Pielak, R. M.; Chou, J.; Griffin, R. G. *J. Am. Chem. Soc.* **2010**, *132*, 10958−10960.
(46) Zhou, D. H.; Rienstra, C. M. *J. Magn. Reson.* **2008**, *192*, 167−172.
(47) Lewandowski, J. R.; Sein, J.; Blackledge, M.; Emsley, L. *J. Am. Chem. Soc.* **2010**, *132*, 1246−1248.
(48) Shaka, A. J.; Keeler, J.; Frenkiel, T.; Freeman, R. *J. Magn. Reson.* **1983**, *52*, 335−338.
(49) Marion, D.; Ikura, M.; Tschudin, R.; Bax, A. *J. Magn. Reson.* **1989**, *85*, 393−399.
(50) Laage, S.; Marchetti, A.; Sein, J.; Pierattelli, R.; Sass, H. J.; Grzesiek, S.; Lesage, A.; Pintacuda, G.; Emsley, L. *J. Am. Chem. Soc.* **2008**, *130*, 17216−17217.
(51) Emsley, L.; Bodenhausen, G. *Chem. Phys. lett.* **1990**, *165*, 469−476.
(52) Barbet-Massin, E.; Pell, A. J.; Jaudzems, K.; Franks, W. T.; Retel, J. S.; Kotelovica, S.; Akopjana, I.; Tars, K.; Emsley, L.; Oschkinat, H.; Lesage, A.; Pintacuda, G. *J. Biomol. NMR* **2013**, *56*, 379−386.
(53) Pawson, T.; Schlessinger, J. *Curr. Biol.* **1993**, *3*, 434−442.
(54) Bjorkman, P. J.; Saper, M. A.; Samraoui, B.; Bennett, W. S.; Strominger, J. L.; Wiley, D. C. *Nature* **1987**, *329*, 506−512.
(55) Klovins, J.; Overbeek, G. P.; van den Worm, S. H. E.; Ackermann, H. W.; van Duin, J. *J. Gen. Virol.* **2002**, *83*, 1523−1533.
(56) Holsinger, L. J.; Nichani, D.; Pinto, L. H.; Lamb, R. A. *J. Virol.* **1994**, *68*, 1551−1563.
(57) Fajardo, D. A.; Cheung, J.; Ito, C.; Sugawara, E.; Nikaido, H.; Misra, R. *J. Bacteriol.* **1998**, *180*, 4452−4459.

(58) Hu, K. N.; Qiang, W.; Tycko, R. *J. Biomol. NMR* **2011**, *50*, 267−276.
(59) Schmidt, E.; Gath, J.; Habenstein, B.; Ravotti, F.; Szekely, K.; Huber, M.; Buchner, L.; Bockmann, A.; Meier, B. H.; Guntert, P. *J. Biomol. NMR* **2013**, *56*, 243−254.
(60) Nielsen, J. T.; Kulminskaya, N.; Bjerring, M.; Nielsen, N. C. *J. Biomol. NMR* **2014**, *59*, 119−134.
(61) Moseley, H. B.; Sperling, L. J.; Rienstra, C. M. *J. Biomol. NMR* **2010**, *48*, 123−128.
(62) Ernst, R. R.; Bodenhausen, G.; Wokaun, A. *Principles of Nuclear Magnetic Resonance in One and Two Dimensions*; Clarendon: Oxford, UK, 1987.